



Photocatalytic properties of zirconium oxide–zinc oxide nanoparticles synthesised using microwave irradiation

Olga Długosz¹ · Krzysztof Szostak¹ · Marcin Banach¹

Received: 2 August 2019 / Accepted: 27 August 2019 / Published online: 6 September 2019
© The Author(s) 2019

Abstract

ZrO₂–ZnO nanoparticles with different mass concentrations of ZrO₂ (1%, 5%, 10%, 20%) were prepared using a two-stage precipitation method with microwave irradiation. The ZrO₂–ZnO with 10% of ZrO₂ had the highest photocatalytic activity. The obtained material was characterised using XRD, which confirmed a high crystal structure in the synthesised material, and transmission electron microscopy (TEM) analysis, which depicted that micro and nano needle-shaped particles had been obtained and that irregularly shaped nanoparticles were present on the surface of those particles. TEM–EDX analysis confirmed the presence of both ZnO and ZrO₂ in the product. FT-IR analyses showed that the positions of peaks related to Zn–O and Zr–O absorption bands did not change in ZrO₂–ZnO NPs. The initial concentration of Methylene Blue (MB), the pH of the solution, and the mass of the photocatalyst were investigated to determine the photocatalytic efficiency of the material and the degree of removal of the MB. The highest efficiency (97%) was obtained in the following conditions: 30 mg/dm³ of the MB solution, pH 9 and 70 mg ZrO₂–ZnO after 30 min of reaction time under UV irradiation.

Keywords Zinc oxide · Zirconium oxide · Nanoparticles · Photocatalytic properties · Methylene Blue · Microwave irradiation

Introduction

Oxide semiconductor nanomaterials are gaining increasing interest due to their attractive functional properties related to their small particle size and hence large active surface (Dal Santo et al. 2018; Sowik et al. 2019). Among these features, the photocatalytic properties are of particular interest. This is due to the fact that these kinds of nanomaterials can be used in many fields such as wastewater treatment or coating materials (Ruiz-Hitzky et al. 2019).

Zinc oxide, especially on a nanometric scale, is a low cost, environmentally friendly with potentially high photocatalytic properties (Lakshmi et al. 2012; Lu et al. 2017). ZnO has a broader energy gap (3.2 eV) compared to TiO₂, which directly contributes to lower photocatalytic activity (Nagao et al. 2016). The modification of the structure of ZnO nanoparticles (ZnO NPs) with the addition of metal and

metal oxide nanoparticles affects the distance between the conduction band and the valance band, which may improve the photocatalytic properties of the material (Karuppaiah et al. 2019).

The main limitations of the photocatalytic properties of ZnO nanoparticles are the relatively broad energy gap and the rapid recombination of electron–hole pairs, which limits the photocatalytic activity of ZnO NPs. It has been noted that the addition of metal oxides improves the photocatalytic properties of, among others, ZnO, TiO₂, MgO, WO₃ and SnO₂ in both UV and visible light (Thirumalai et al. 2017; Reszczyńska et al. 2015; Al-Hamdi et al. 2015; Kokorin et al. 2018). One material that enhances the photocatalytic properties of ZnO NPs is zirconium oxide (ZrO₂).

Zirconium oxide belongs to the group of semiconductor materials. It usually occurs in an amorphous form with a relatively wide energy gap [~5.25 eV (Oluwabi et al. 2018)]. Pure ZrO₂ has very limited photocatalytic properties, but the addition of the oxide in the other oxides, including TiO₂, SnO₂, ZnO has beneficial effect on their photocatalytic activity (Aghabeygi et al. 2017; Pirzada et al. 2015). One of the mechanisms to improve properties of photocatalytic oxides is the modification their structure by creating numerous

✉ Olga Długosz
odlugosz@chemia.pk.edu.pl

¹ Faculty of Chemical Engineering and Technology, Institute of Chemistry and Inorganic Technology, Cracow University of Technology, Warszawska 24, 31-155 Cracow, Poland

surface defects, developing the surface of the deposition of other oxide nucleation, thus supporting the electron transfer processes accompanying the photocatalytic process (Uribe López et al. 2019). In the case of the ZrO_2 -ZnO system, in a two-stage process, ZnO particles are obtained on the surface of the amorphous ZrO_2 particles, which may have a different structure than those obtained in a single-stage process (Ibrahim 2015). Additionally, the structure of ZrO_2 plays an important role in the reduction of the electron-hole recombination of doped systems (Gurushantha et al. 2017). The replacement of Zn^{2+} with Zr^{4+} disturbs the charge balance. The disturbed charge balance contributes to the adsorption of more hydroxide ions at the catalyst surface, which additionally blocks the recombination of electron-hole pairs (Karuppaiah et al. 2019). Aghabeygi and Khademi-Shamami (2018) investigated ZnO/ ZrO_2 nanocomposites prepared with ultrasonic irradiation. The ZnO nanocomposite was excited by the transfer of the electrons promoted from the conduction band of ZnO- ZrO_2 and simultaneously transferred the holes from the valence band of ZrO_2 to the ZnO.

There are known methods for obtaining zinc oxide nanoparticles modified by ZrO_2 or other compounds. The great limitations in the proposed tests are the long time of the photodegradation process and the low concentration of dyes used in the processes. Sapawe et al. received ZnO- ZrO_2 -HY zeolite nanocomposite, for the removal of Methylene Blue. The dye removal efficiency was 99.7%, but the dye concentration was 10 mg/dm³, and the process was carried out for 90 min (Sapawe et al. 2013). Chen et al. obtained ZnO modified with SnO₂ nanoparticles to remove various dye wastewaters. By increasing the initial concentration of Congo Red from 20 to 40 ppm, the photodegradation time increased from 40 to 80 min while reducing the efficiency from 96.8 to 89.3% (Chen et al. 2015). These are the reasons why it is necessary to dilute the dye solution, use larger masses of photocatalyst or extend the processing time.

Metal oxide nanoparticles can be obtained by hydrothermal processes usually carried out by several hours. Qui et al. they received doped ZrO_2 -ZnO photocatalyst; however, the process was carried out under pressure reactor for 12 h (Qui et al. 2018). Aghabygi and Khademi-Shamami developed an alternative method of obtaining ZnO/ ZrO_2 nanocomposite using ultrasound, but after 30 min of ultrasonication, the material was calcined (Aghabeygi and Khademi-Shamami 2018). Insertion of the energy into the system using microwave radiation reduces the synthesis time. In addition, the amount of energy in the process allows obtaining products with a high degree of crystallinity, so that the calcining process can be omitted.

This study aimed to prepare ZrO_2 -ZnO nanoparticles using a precipitation method with microwave irradiation. The photocatalytic properties of the obtained material were investigated for the degradation of Methylene Blue (MB)

solution under UV irradiation. The effects of the mass concentration of ZrO_2 in ZnO- ZrO_2 NPs, the initial concentration of MB, the pH of the solution, and the mass of photocatalyst were investigated.

Experimental

Materials

Zinc sulphate $ZnSO_4 \cdot 5H_2O$ (Sigma Aldrich), zirconyl chloride $ZrOCl_2 \cdot 8H_2O$ (Sigma Aldrich) and sodium carbonate Na_2CO_3 (Sigma Aldrich) were used in the synthesis of the photocatalytic material. MB was purchased from Sigma Aldrich and used to study the photocatalytic properties of ZrO_2 -ZnO. All chemicals were of analytical grade and were used without further purification.

Synthesis of ZrO_2 -ZnO

A precipitation method was used to produce ZrO_2 -ZnO. Two-step synthesis was carried out in a microwave reactor. First, $Zr(OH)_4$ was synthesised by mixing 20 ml 1 M $ZrOCl_2 \cdot 8H_2O$ with 20 ml 2 M Na_2CO_3 . The suspension was transferred to a Teflon vessel and it was heated in a MAGNUM II microwave reactor (Ertec, Poland) for 10 min at 150 °C. The obtained zirconium oxide(IV) was filtered and dried at 70 °C for 24 h. In the next step, solid ZrO_2 nanoparticles in an amount corresponding to fixed percentage composition, 20 ml of 1 M $ZnSO_4 \cdot 5H_2O$ and 10 ml of 2 M Na_2CO_3 were added to the beaker. After mixing, the suspension was transferred to a Teflon vessel and heated in the microwave reactor for 10 min at 180 °C. The obtained product was filtered and dried at 70 °C for 24 h. The effect of the ZrO_2 mass on the photocatalytic properties of the final product was also established.

Instrumental analysis

The structure of ZrO_2 -ZnO before and after the photocatalytic reaction was examined using transmission electron microscopy (TEM) with energy dispersive X-ray analysis (EDX) and elemental mapping using a Tecnai Transmission Electron Microscope, F20 X-Twin, FEI Europe. The Fourier Transform Infrared Spectroscopy (FTIR) method (Nicolet 380) was helpful for determining the degree of sorption of the dye as well as its decomposition under the influence of UV. XRD analysis (Philips X'Pert camera with monochromator PW 1752/00 $CuK\alpha$) determined the degree of crystallinity of ZrO_2 , ZnO and ZrO_2 -ZnO.

Optical studies

The spectrum of MB and its concentration were examined by UV–Vis spectroscopy (Rayleigh UV-1800 spectrophotometer). The calibration curve was prepared at 664 nm and was made in triplicate (Fig. 1).

The absorption, which corresponds to the energy difference between the top of the valence band and the bottom of the conduction band, is defined to designate the band gap using the UV–Vis method (Mexicana De Física et al. 2007). The value of the band gap (E_g) energy was obtained using the following equation:

$$E_g = \frac{h \cdot c \cdot 10^{19}}{\lambda \cdot 1.6} [\text{eV}], \tag{1}$$

where h —Planks constant = $6.626 \cdot 10^{-34}$ J s, c —speed of light = $3.0 \cdot 10^8$ m/s, λ —cut off wavelength/absorption edge in nm.

Photocatalytic degradation experiments

The photodegradation of MB using $\text{ZrO}_2\text{-ZnO}$ was studied using batch mode experiments. This was done by studying the effect of initial concentration of dye, material dose and pH of the solution. The photocatalytic activities of the

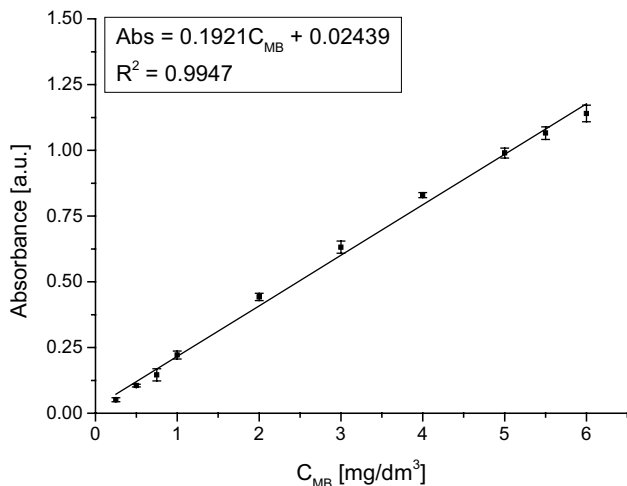


Fig. 1 Calibration curve for MB absorption at 664 nm

Table 1 Experimental range and levels of independent process variables

Variable	Unit	Notation	Range				
			$-\alpha$ (−1.68)	(−1)	(0)	(1)	$+\alpha$ (+1.68)
Initial concentration of MB	C_0 (mg/dm ³)	x_1	23.18	30	40	50	56.82
pH	pH (−)	x_2	3.64	5	7	9	10.36
Photocatalyst mass	m (g)	x_3	16.36	30	50	70	83.64

photocatalyst were investigated by measuring the degradation of MB aqueous solutions under UV light irradiation using a UV lamp (wavelength 360 nm). A certain amount of the material was added while mixing 30 ml of the solution of dye with a magnetic stirrer for a specified period of time. The amounts of the degraded dye R_D (mg/g) (2) and efficiency of photocatalytic degradation of MB (3) were calculated from the following dependences:

$$R_D \text{ (mg/g)} = \frac{(C_0 - C_t)V}{m}, \tag{2}$$

$$E \text{ (%) } = \frac{(C_0 - C_t)}{C_0} \cdot 100, \tag{3}$$

where C_0 and C_t are the initial and final concentrations of the dye solution (mg/dm³) at time t , V is the solution volume (dm³), and m is the mass of the material (g).

Statistical analysis

The initial concentration of the dye was tested using a UV–Vis spectrophotometer in the range of 20–60 mg/dm³. The effect of the mass of the photocatalytic deposit was examined in the range of 10–50 mg and the effect of the pH of the solution was tested in the range from 3 to 11. The pH of the solution was adjusted with 15% HNO₃ or 0.1 M NaOH. A central composite design (CCD) plan was used to examine the effect of parameters on the photocatalysis process and determine the most favourable parameter values (Table 1). As the output parameters, the degree of dye removal per 1 g of the deposit and photodegradation efficiency were used. The research results were developed using the program STATISTICA (version 10.0).

Results and discussion

Selection of the final deposit based on the photocatalytic activity of the product

In the first stage, to obtain the material with the highest photocatalytic efficiency, the most favourable mass concentration of ZrO_2 in the $\text{ZrO}_2\text{-ZnO}$ nanoparticles was determined. For this purpose, a various mass of ZrO_2 powder and

a constant volume of ZnSO_4 and Na_2CO_3 solutions were added to the beaker. The mixture was transferred to a Teflon vessel and heated using microwave irradiation for 10 min at 180 °C. After the process, the product was filtered, washed and dried. The photodegradation efficiency and the amount of degraded dye of ZrO_2 -ZnO with a mass concentration of ZrO_2 equalling 1%, 5%, 10% and 20% are presented in Fig. 2. The efficiency of pure ZnO and ZrO_2 nanoparticles is also shown. Each material was tested in darkness and in UV light in triplicate. The results of the photocatalytic and sorption studies were used to compare the properties of each deposit.

ZrO_2 -ZnO with 10% ZrO_2 showed the highest photocatalytic activity compared to materials with different concentrations of ZrO_2 . A further increase in the concentration of ZrO_2 increased the sorption capacity of the material but reduced photocatalytic properties, which was undesirable (Fig. 2).

On the basis of the conducted photodegradation studies of MB on pure ZrO_2 , an increase in absorbance at a wavelength of 664 nm was observed during the reaction time of irradiation. Higher absorbance of the solution indicates an increase in the concentration of the dye in the solution. The study of the kinetics of the sorption process confirmed the high impact of physical sorption on the process (Table 2).

The second-order model is a model with the highest determination coefficient, which suggests the chemical nature of sorption. Based on the analysis of the process carried out under UV, the desorption process took place. The second-order model, despite a much lower value of the reaction rate constant is still positive, which would indicate a slow sorption process. In the case of the first-order model, the determination coefficient is lower, especially in the case of the UV process. However, the reaction rate constant is negative, which confirms the desorption process. Both models show some disadvantages in the actual description of the sorption process on ZrO_2 , hence the complex mechanism of the process, combining the dye with the material, both by chemical and physical interactions. The process of desorption under the influence of UV is not yet known, therefore, further research should be carried out.

The constant of the reaction rate in the pseudo-first-order model in the process conducted with UV radiation has a negative value, which confirmed the desorption process. In all kinetic models, the degree of regression fit of experimental data to model equations is high, which suggests a complex process of physical sorption combined with chemical sorption. According to the results, after the first minute of irradiation with UV radiation, an increase in the concentration of MB in the solution was observed (Fig. 3).

Fig. 2 Photocatalytic efficiency of ZrO_2 -ZnO with percentage concentrations of ZrO_2 from 0 to 20%_{wt}

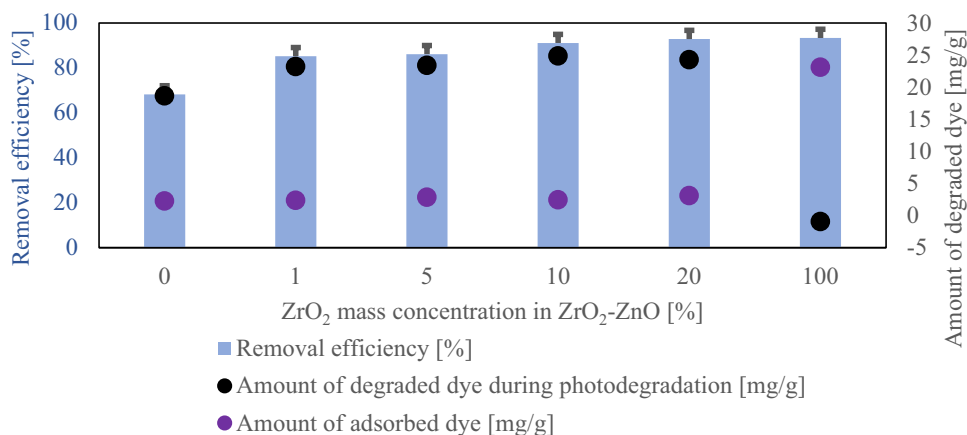


Table 2 Kinetic parameters of MB adsorption onto ZrO_2 in darkness and in UV light

Kinetic model	Parameters	Sorption in the darkness	Sorption under UV
First order kinetic model	k_1 (min^{-1})	0.1181 ± 0.05134	-0.02487 ± 0.003306
	$R_{D\text{max}}$ (mg/g)	5.9265 ± 1.1720	0.9112 ± 0.8889
	R^2	0.9519	0.7281
Second order kinetic model	k_{II} (g/mg/min)	0.06232 ± 0.004051	$1.386 \cdot 10^{-3} \pm 2.985 \cdot 10^{-4}$
	$R_{D\text{max}}$ (mg/g)	28.9855 ± 0.2198	25.8398 ± 0.3849
	R^2	0.9998	0.9991
Elovich	β (g/mg)	0.5304 ± 0.03424	0.6910 ± 0.1976
	R^2	0.9836	0.7535
Experimental data	$R_{D\text{exp}}$ (mg/g)	28.5712	26.9068

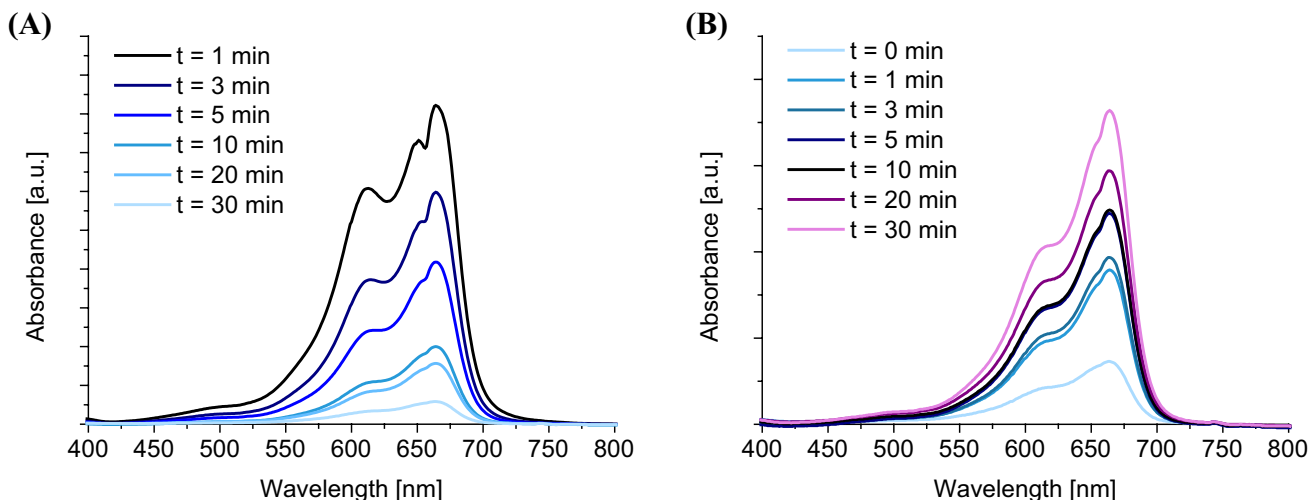


Fig. 3 Absorption spectra of MB solution in sorption onto ZrO₂ in darkness (a) and under UV irradiation (b)

The surface energy of adsorption decreases with increasing temperature. In the case of UV radiation, the energy added to the system may increase the energy of the MB particles and thus reduce the surface energy between the dye particles and the ZrO₂ surface. With a significant contribution of physical sorption, the energy of the bond between the bed and the dye is lower compared to chemical sorption. Therefore, after providing additional energy in the form of UV radiation, MB particles can be desorbed (Fig. 4).

Additionally, for the obtained materials, the width of the energy gap was determined (Table 3). A higher mass ratio of ZrO₂ in ZrO₂-ZnO materials caused a decreased width in the energy gap. The width of the energy gap for each material

was obtained using the UV-Vis method. Absorption, which corresponds to the energy difference between the top of the valence band and the bottom of the conduction band, was used to designate the band gaps (Fig. 5). Based on the studies, material with 10%_wt of ZrO₂ was chosen as the material for further analysis.

Photocatalytic degradation of dye solutions

Effects of parameters processes

A CCD with three factors and five coded levels was adopted in the optimization study. Table 4 presents the

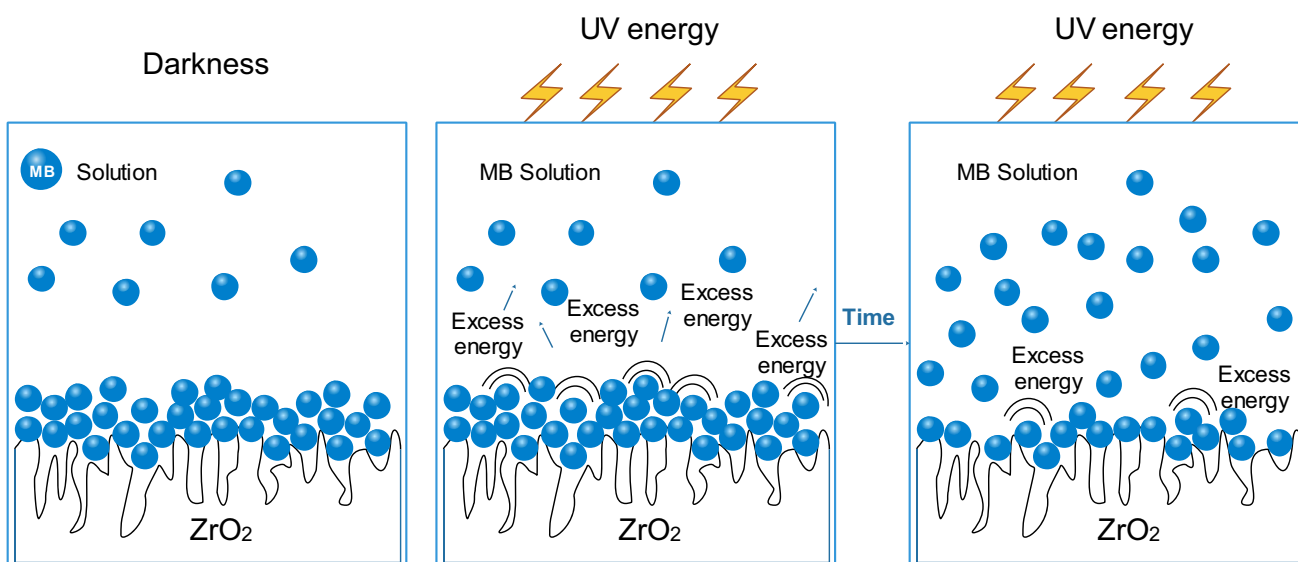
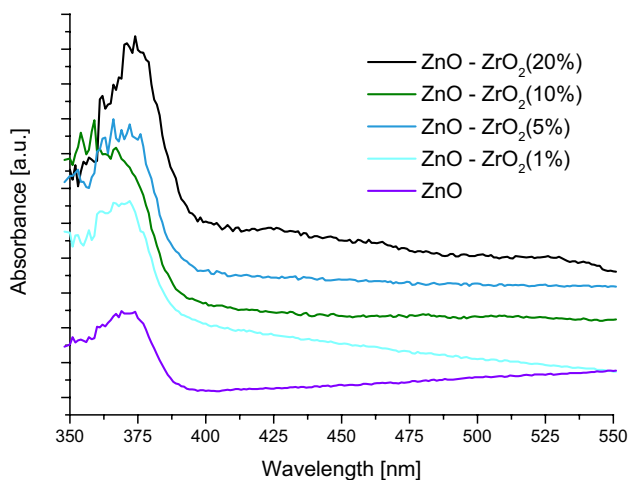


Fig. 4 Desorption mechanism for the MB-ZrO₂ system resulting from UV irradiation

Table 3 Width of band gap for ZnO with ZrO₂

Sample	Width of band gap (eV)	Photodegradation of the dye (mg/g)	Dye reduction in the darkness (mg/g)	The contribution of sorption in the dye degradation process (%)
ZnO	3.18 ± 0.02	16.38 ± 0.49	2.25 ± 0.31	12.09 ± 0.49
ZnO–ZrO ₂ (1%)	3.19 ± 0.02	20.84 ± 0.26	2.37 ± 0.19	10.20 ± 0.28
ZnO–ZrO ₂ (5%)	3.18 ± 0.01	20.55 ± 0.23	2.84 ± 0.94	12.14 ± 0.72
ZnO–ZrO ₂ (10%)	3.17 ± 0.01	22.39 ± 0.18	2.46 ± 0.19	9.89 ± 0.23
ZnO–ZrO ₂ (20%)	3.17 ± 0.02	22.19 ± 0.03	3.09 ± 0.46	12.21 ± 0.30
ZrO ₂	~ 5.25 (Oluwabi et al. 2018)	– 1.05 ± 0.42	23.10 ± 0.15	100.0 ± 0.35

**Fig. 5** Optical absorption edge determination for ZrO₂–ZnO with different concentration of ZrO₂

experimental values of the photocatalytic efficiency of MB degradation and the amounts of the degraded dye under designed conditions. The response variable was fitted using a regression model:

$$y = a_0 + \sum_{i=1}^k a_i \cdot x_i + \sum_{i=1}^k a_{ii} \cdot x_i^2 + \sum_{i < j} a_{ij} \cdot x_i \cdot x_j, \quad (4)$$

where y —efficiency of photodegradation (%), a_0 —constant term, a_i —linear coefficients, a_{ii} —quadratic coefficients, a_{ij} —coefficient of the interaction parameters, x_i, x_j —values of the independent variables.

Based on the ANOVA results, parameters that significantly affected the photocatalytic efficiency of ZrO₂–ZnO were determined (Table 5). All selected input variables as well as their interactions had a significant effect on the photocatalytic properties of the material. The p value of 0.05 was determined as the significance level in the analysis.

The increase in the gradient between the amount of ZrO₂–ZnO and the dye in the system contributed to the

Table 4 Experimental results of the CCD plan for the ZrO₂–ZnO photocatalytic process

Lp.	C_0 (mg/dm ³)	Mass (mg)	pH (–)	E (%)	R_D (mg/g)
	x_1	x_2	x_3	y_1	y_2
1	30	30	5	62.77	20.12
2	30	70	5	66.03	8.98
3	30	30	9	86.99	28.12
4	30	70	9	97.15	13.24
5	50	30	5	54.89	28.74
6	50	70	5	63.49	14.48
7	50	30	9	67.40	35.66
8	50	70	9	90.64	20.70
9	23.18	50	7	95.63	13.91
10	56.82	50	7	79.67	28.69
11	40	50	3.64	70.78	17.14
12	40	50	10.38	91.15	22.47
13	40	16.36	7	64.59	48.29
14	40	83.64	7	96.14	14.05
15	40	50	7	88.16	21.62
16	40	50	7	88.95	21.75

increase in the removal rate of MB from the solution, which is associated with an increase in driving force. The initial concentration of the dye as a factor with a negative coefficient estimate caused a decrease in the efficiency of the ZrO₂–ZnO together with an increase in the concentration of dye in the system (Fig. 6). Lee et al. studied the effect of various factors on ZnO efficiency, also confirming the negative effect of the initial concentration of dye and a positive coefficient estimate of the pH of the solution on the degradation of phenoxyacetic acid (Lee et al. 2015).

Effect of initial dye concentration on photocatalytic performance

The photocatalytic degradation of MB was carried out at different initial concentrations of dye in the range of 20–60 mg/dm³. The results are shown in Fig. 7. An increase in the concentration of dye decreases the path length of photons entering the pollutant solution. At high pollutant concentrations, a significant amount of light may be absorbed

Table 5 Coefficient of regression model and its significance on deposit efficiency (%) and dye removal rate (mg/g)

Independent variables	Symbol	E (%)				R_D (mg/g)			
		Coefficient estimate	Std. deviation	F value	p value	Coefficient estimate	Std. deviation	F value	p value
Mean/constant		89.41	0.3957	62.40	0.0028	21.97	0.0665	330.4	0.0019
(1) C_0 [mg/dm ³] (L)	x_1	-15.61	0.5109	-30.55	0.0208	13.30	0.0859	154.9	0.0041
C_0 [mg/dm ³] (Q)	x_1^2	-13.63	1.043	-13.07	0.0486	-4.705	0.1753	-26.84	0.0237
(2) m [mg] (L)	x_2	24.21	0.5109	47.39	0.0134	-27.79	0.0859	-323.7	0.0020
m [mg] (Q)	x_2^2	-28.21	1.043	-27.05	0.0235	15.04	0.1753	85.78	0.0074
(3) pH [-] (L)	x_3	31.85	0.5107	62.36	0.0102	8.467	0.0858	98.64	0.0065
pH [-] (Q)	x_3^2	-27.00	1.043	-25.89	0.0246	-7.689	0.1752	-43.86	0.0145
1L by 2L	$x_1 \cdot x_2$	13.02	1.123	11.60	0.0547	-2.264	0.1887	-12.00	0.0529
1L by 3L	$x_1 \cdot x_3$	-11.09	1.122	-9.881	0.0642	0.6271	0.1886	3.325	0.1860
2L by 3L	$x_2 \cdot x_3$	15.22	1.122	13.57	0.0468	-3.138	0.1886	-16.64	0.0382

Italic values indicate significance of p value ($p < 0.05$)

L—linear main effects of input values

Q—square main effects of input values

1L by 2L linear interactions effects between C_0 and m

1L by 3L linear interactions effects between C_0 and pH

2L by 3L linear interactions effects between m and pH

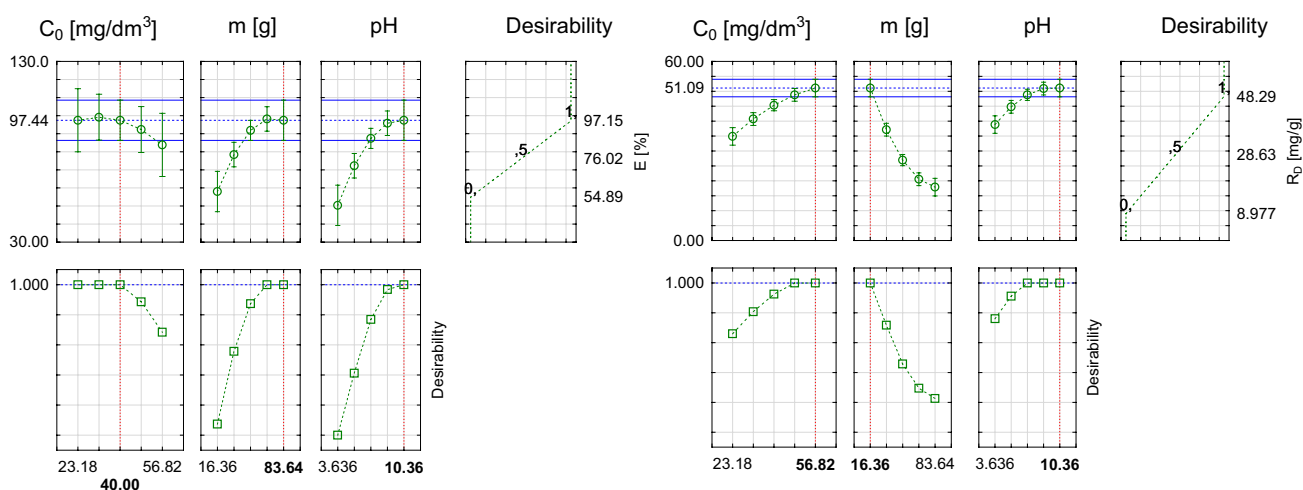


Fig. 6 Optimization plot for the removal of MB by ZrO_2-ZnO (10% ZrO_2)

by the pollutant molecules rather than the catalyst, and this reduces catalytic efficiency. For the degree of dye removal, constant bed weight and higher MB concentration increases the concentration gradient of active reagents. A greater driving force improves the degree of dye removal from the solution. Similar results were obtained by investigating the effectiveness of ultrasonicated $ZnO-ZrO_2$ on another dye, congo red (Aghabeygi and Khademi-Shamami 2018), and by testing MB on ZnO modified SnO_2 (Lin et al. 2018).

The effect of photocatalyst content on the photocatalytic performance The amount of catalyst was one of the most effec-

tive parameters in the degradation studies. This was due to the increase in the number of ZnO particles, which increased the adsorption of photons and adsorption of pollutant molecules. On the other hand, the concentration gradient between the bed and the dye was the highest for 10 mg of the bed. The degree of dye removal, unlike efficiency, is referred to a unit mass of the bed used, hence an increase in the amount of ZrO_2-ZnO causes a decrease in the use of the bed surface. It has been observed that with the increase of ZrO_2-ZnO (10–90 mg), the efficiency of the deposit increases, which is in contrast to the degree of dye removal. With a higher amount of photocatalyst mass, the number of free electron-hole pairs increases, there-

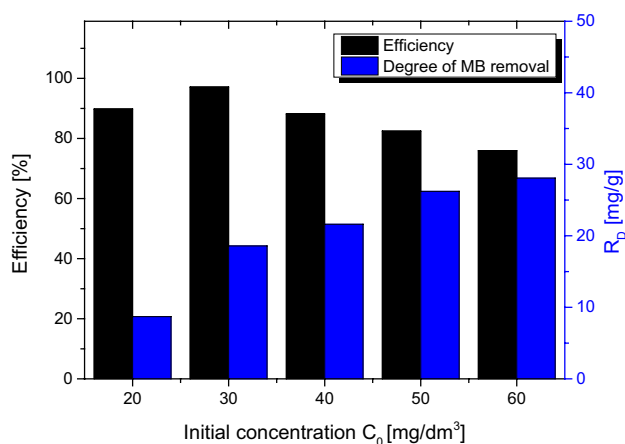


Fig. 7 Effect of the initial concentration of MB solution on the efficiency and photodegradation of MB on ZrO_2 -ZnO ($m = 50$ mg, $pH = 7$)

fore, more particles of the dye are removed. However, not all active spaces of the ZrO_2 -ZnO are used (Fig. 8). In the case of deposit efficiency, the concentration gradient increases, which results in a higher degree of dye removal without this being converted into a unitary amount of dye in the solution.

Effect of the initial pH of the dye solution on photocatalytic performance At the acidic pH of the solution, the lowest degree of oxidation and the lowest degree of dye removal from the solution were observed (Fig. 9). Spathis and Poulivos showed that in aqueous solutions, under the influence of UV irradiation, ZnO can undergo partial dissolution, which is known as photocorrosion (Spathis and Poulivos 1995). In an acidic environment, it can proceed as follows:

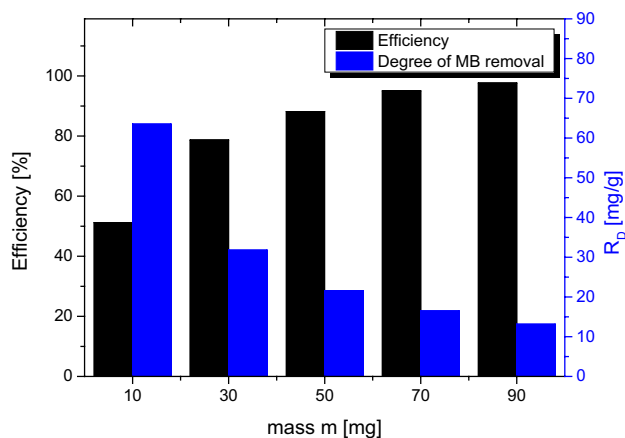
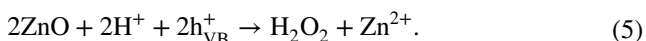


Fig. 8 Effect of mass on efficiency and photodegradation of MB on ZrO_2 -ZnO ($C_0 = 40$ mg/dm³, $pH = 7$)

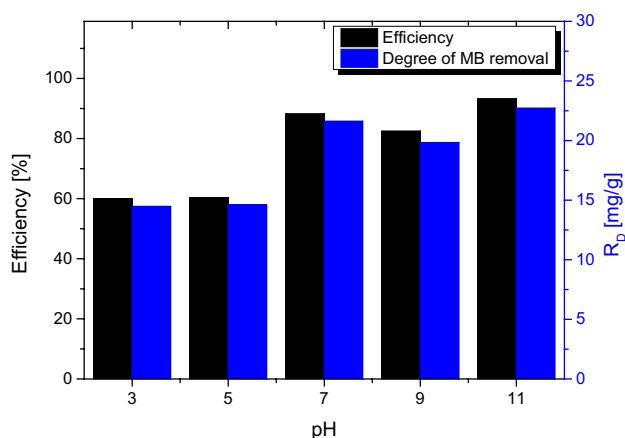
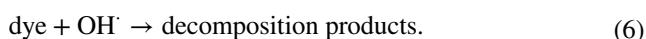


Fig. 9 Effect of solution pH on efficiency and photodegradation of MB on ZrO_2 -ZnO ($C_0 = 40$ mg/dm³, $m = 50$ mg)

This results in a double inhibition of the photocatalytic activity of the material. First, it reduces the amount of zinc oxide that would generate electron–hole pairs. Additionally, a part of h_{VB}^+ , instead of participating in the generation of H^+ , can participate in the competitive ZnO oxidation reaction and thus reduce the overall efficiency of the photocatalytic process. In solutions with a higher pH near the Zn^{2+} ions, mainly H_2O and OH^- ions (H_2O_{ads} , OH^-_{ads}) are absorbed. They can be oxidised by h_{VB}^+ , which is generated under the influence of UV radiation (Aghabeygi and Khademi-Shamami 2018). The OH^- radicals can participate in further free radical reactions with dye particles adsorbed on the ZnO surface. This leads to the degradation of organic compounds:



Kinetic studies, effect of time on photocatalytic performance

In the general approach, the mechanism of photocatalytic degradation follows the Langmuir–Hinshelwood (L–H) kinetic model (Lee et al. 2015). The L–H model was used to investigate the effect of time on the heterogeneous photodegradation process and the equation of reaction rate (r) is represented by

$$r = \frac{K_1 K_2 C}{1 + K_2 C}, \quad (7)$$

where K_1 is the rate constant, which includes various parameters such as nanophotocatalyst content, and K_2 is the adsorption constant. After assuming that the dye concentration is low, $K_2 C \ll 1$, hence the reaction rate is a

first-order equation (Aghabeygi and Khademi-Shamami 2018). Taking into account the boundary conditions [$C = C_0$ at t (time) = 0], it is possible to determine the reaction rate constant:

$$-\ln \frac{C}{C_0} = kt, \quad (8)$$

where k is the photodegradation rate constant (min^{-1}).

A series of tests were carried out where the concentration of the dye in the solution was examined at a concentration of MB 40 mg/dm^3 with 500 mg of photocatalyst in 300 ml of mixture. The results are shown in Fig. 10. For the first 30 min, to establish the equilibrium, the process was carried out in darkness. After selected intervals, a sample was taken to examine the concentration of the dye. The convex curve indicates a decreasing amount of dye in the mixture and, consequently, the dye particles are degraded with a lower rate. It can be seen from Fig. 10b that the kinetic experimental data are in good agreement with the kinetic model ($R^2 = 0.9925$) and the first-order rate constant equals 0.03324 min^{-1} . Belcha et al. examined the effect of catalyst concentration on the MB degradation rate over time. They determined rate constants of 0.0124 min^{-1} for ZnO NPs obtained using the sol–gel method and 0.0084 min^{-1} for ZnO NPs obtained using the precipitation method (Balcha et al. 2016). Payra et al. investigated the photocatalytic degradation mechanism of MB over ZIF-derived ZnO, obtaining first-order kinetics and a rate constant of 0.0452 min^{-1} , which confirmed the efficiency of the photocatalytic material (Payra et al. 2019).

Characterization

TEM–EDX investigations TEM analysis confirms that ZrO_2 –ZnO NPs preserve their original structure after sorption and photocatalytic processes (Fig. 11a–f). Different types of particles were obtained. Long needle-shaped microparticles as well as their nanoscale counterparts were observed (Fig. 11a, c, e). At the same time, irregularly shaped nanoparticles consisting of crystallites of several nanometers appear on the surface of other particles (Fig. 11b, d, f). An EDX analysis was also carried out to confirm the elemental composition of the obtained composite (Fig. 12). The EDX analysis confirmed the presence of all three elements: Zr, Zn and O. It can be seen that in the first area of scanning, there are sharp peaks from zinc and oxygen indicating the presence of ZnO, however, there are no visible reflexes from zirconium. In contrast to the first area, in the second scanning region, clear peaks are visible from both zinc and zirconium as well as oxygen, which confirms the presence of ZrO_2 and ZnO. Depending on the place of sample analysis, the material composition differs from 0.54 to 24.41%_{wt} ZrO_2 . Compared to the results, the percentage composition of the XRD analysis was 10–11%_{wt} ZrO_2 . A discrepancy in the results indicates the inhomogeneity of the material in the nanoscale, nonetheless, it was expected that both the use of powdered ZrO_2 and the use of only 10% of ZrO_2 on the whole mass would prevent a homogeneous material for the entire volume from being obtained.

XRD investigations XRD analysis confirmed that zinc oxide in crystalline form and amorphous zirconium oxide had been obtained. Materials after sorption and photodegradation processes did not change their form. Figure 13 shows the XRD patterns of the synthesized pure ZnO, ZrO_2 and

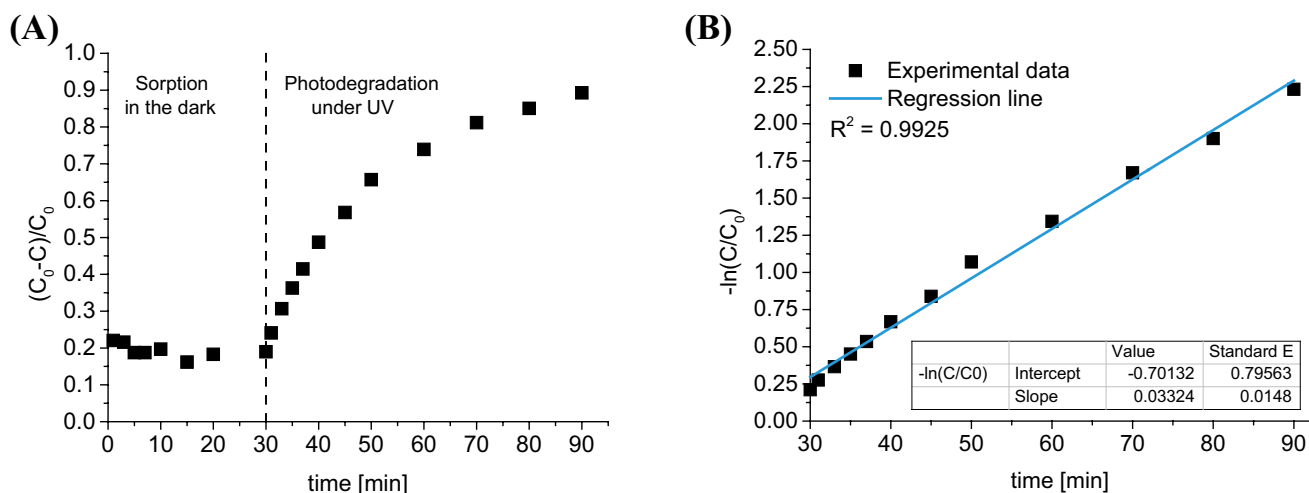


Fig. 10 Absorption of MB in different exposure times under UV radiation (a); kinetics of photocatalyst degradation of MB under UV radiation (b)

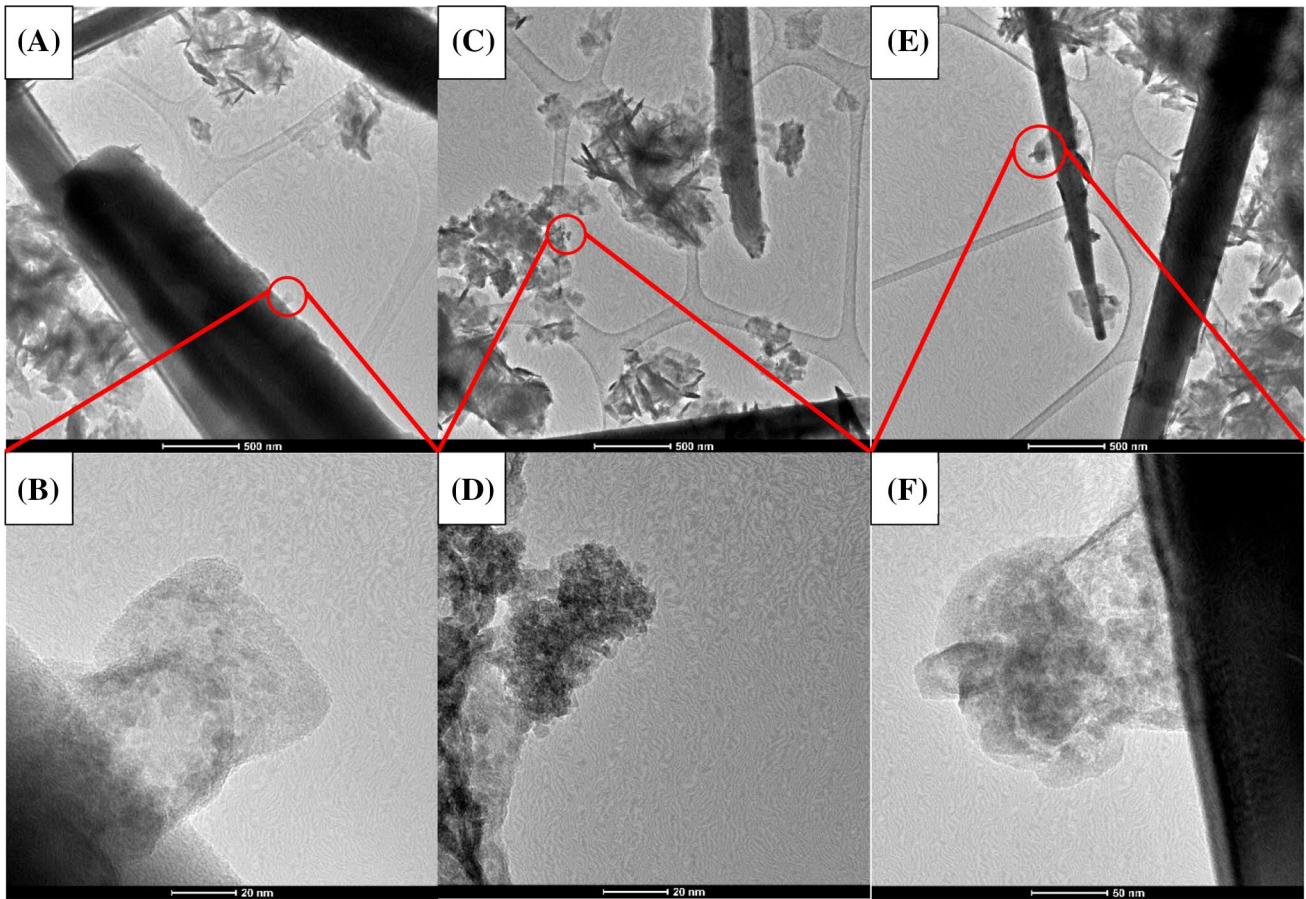


Fig. 11 TEM images of the ZrO_2 -ZnO nanoparticles: pure ZrO_2 -ZnO (a, b), after the sorption process (c, d), after the photocatalytic process (e, f)

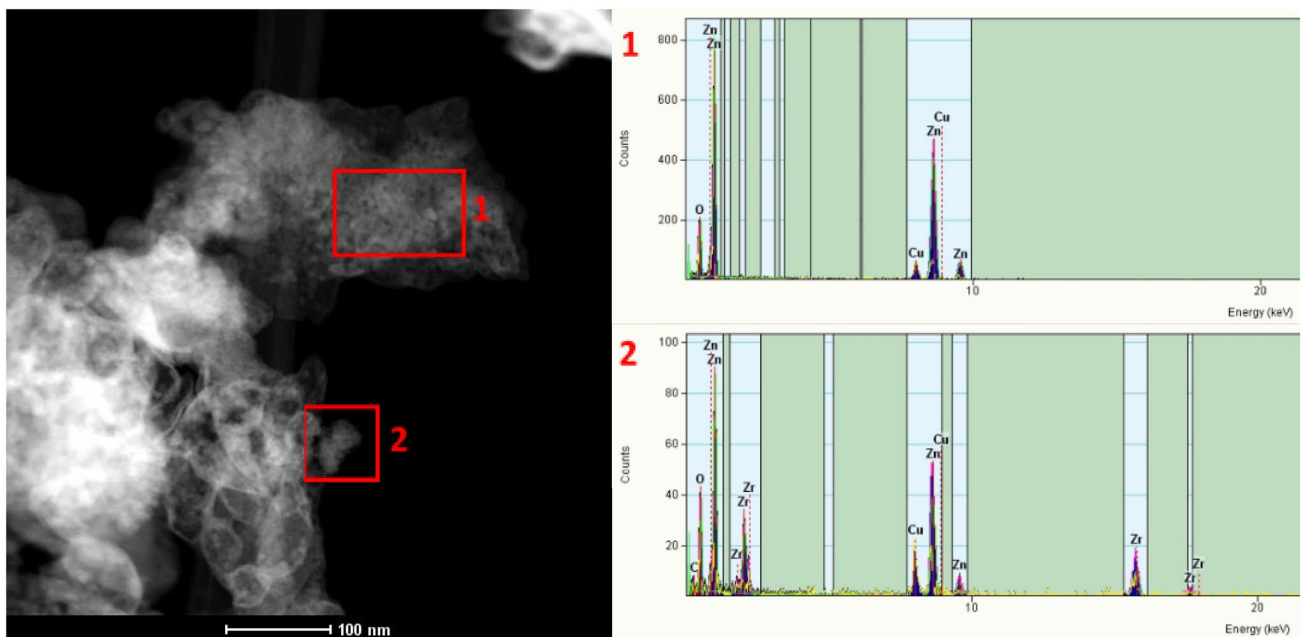


Fig. 12 TEM-EDX images of the ZrO_2 -ZnO nanoparticles

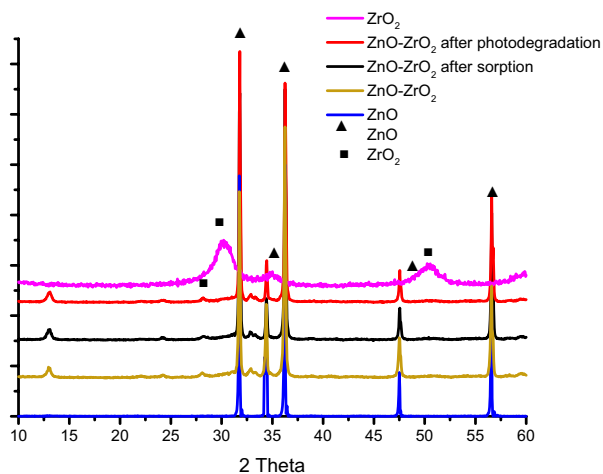


Fig. 13 XRD pattern of ZnO, ZrO₂, and ZrO₂-ZnO (10%) before and after sorption and photodegradation processes

ZrO₂-ZnO (10%) before and after the sorption process and the photodegradation of the MB. The XRD pattern of the prepared crystalline ZnO is in accordance with the hexagonal zincite crystalline structure of ZnO, with sharp and strong peaks at 2θs of 31.75°, 34.40°, 36.24°, 47.54° and 56.61°, which correspond to (100), (002), (101), (012) and (110), respectively (Garino et al. 2019; Hasanpoor et al. 2015). The XRD pattern for pure ZrO₂ confirmed characteristic planes at 2θs of 30.23°, 34.92° and 50.26° (Singh and Nakate 2014; Manjunatha and Dharmaprakash 2016). The peak centred at 30.23° (101) is characteristic of the tetragonal crystalline phase (Uribe López et al. 2019). In the ZrO₂-ZnO, the corresponding peaks of ZrO₂ are absent, whereas peaks corresponding to the ZnO remain sharp and strong. In addition, the diffractograms representing ZnO-ZrO₂ show less homogeneous patterns compared to pure ZnO, which indicates an increased amorphous structure. The patterns suggest a greater polydispersity of the material surface, thanks to which the material has better photocatalytic properties.

FTIR results The FT-IR spectra of pure ZnO, pure ZrO₂ and ZnO-ZrO₂ nanoparticles are presented in Fig. 14. All materials show spectra at a wavenumber of about 500 cm⁻¹, which indicates the metal-oxygen bonding of Zn-O and Zr-O (Janaki et al. 2015). The peaks at around 3400 cm⁻¹ and 1500 cm⁻¹ in all samples are the stretching and bending vibrational bands of the hydroxyl groups adsorbed on the surface. These effects from hydroxyl groups are strongly visible due to the lack of calcination of the obtained products. At the same time, it should be noted that these interactions are more pronounced for samples with ZrO₂, which is related to the amorphous nature of these products and the formation of bonds between O-H and Zr-O (Zinatloo-

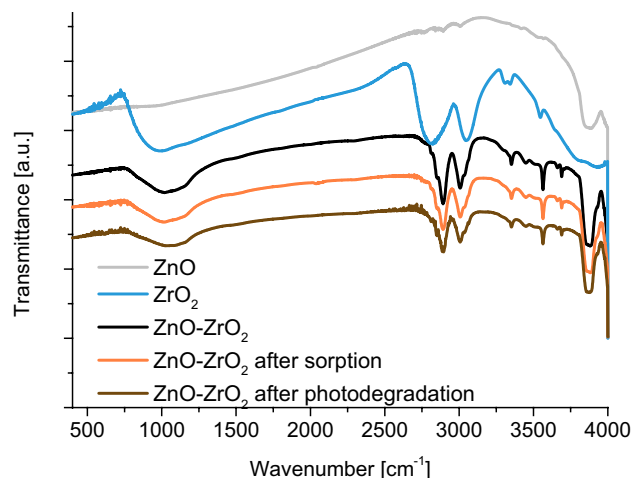
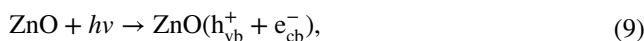


Fig. 14 FT-IR spectra of ZnO, ZrO₂, and ZrO₂-ZnO (10% ZrO₂) before and after sorption and photodegradation processes

Ajabshir and Salavati-Niasari 2016). The sharp signals in the region of 1360–1420 cm⁻¹ appear from carbonate anions, which is a direct result of the use of sodium carbonate as a precipitating agent (Khan et al. 2016). There are no visible peaks derived from adsorbed MB at 1390, 1487 or 1590 cm⁻¹ (Bartošová et al. 2017) in the ZnO-ZrO₂ after the sorption process due to the fact that they coincide with the peaks from pure bed in the region of 1360–1600 cm⁻¹, which in combination with a relatively small amount of adsorbed MB, causes them to be totally covered.

Mechanism of photocatalyst

The mechanism of dye photodegradation using a ZnO semiconductor initiated by UV can be presented in the following equation:



where h_{vb}^+ are holes of the generated valence band of the semiconductor, which have strong oxidising properties, and e_{cb}^- are electrons generated in the conduction band of the semiconductor, which have high reducing properties (Uribe López et al. 2019).

The addition of semiconductors is one way of improving the photocatalytic properties of ZnO. Different widths of energy bands occurring in both oxides contribute to reducing the distance between the conduction bands and the valence bands in the whole composite. In the ZrO₂-ZnO system, some of the electrons pass from the conduction band of ZrO₂ to the conduction band of ZnO. At the same time, from the valence band of ZnO, some of the holes migrate to the valence band of ZrO₂, leading to the generation of electron-hole pairs (Fig. 15). Electron transfer, and consequently

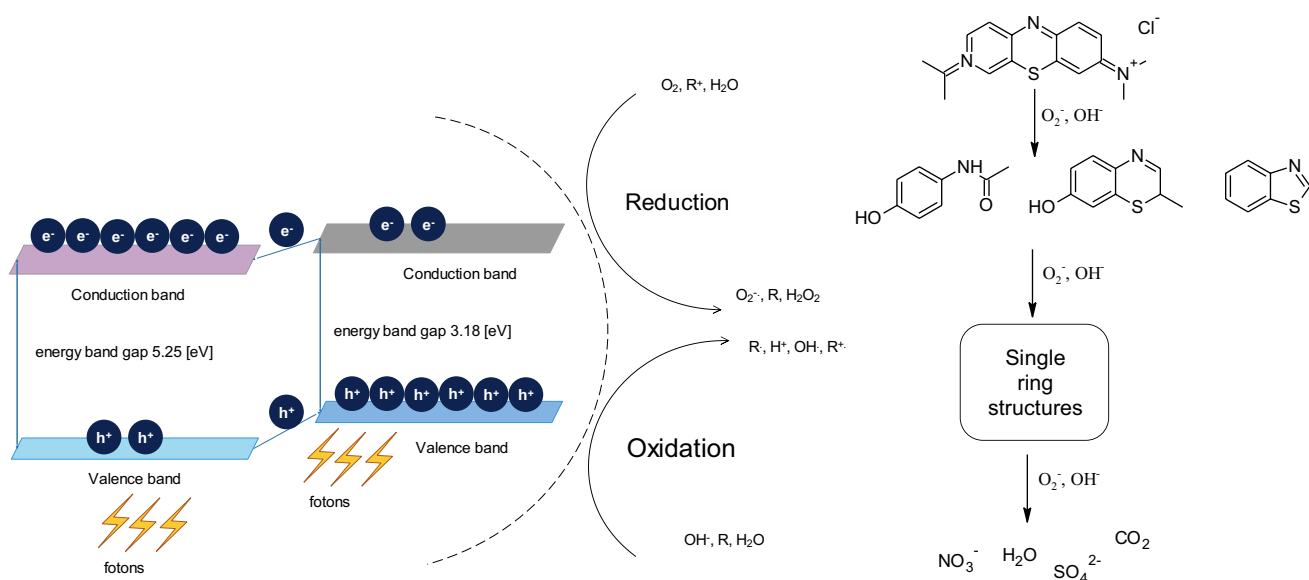


Fig. 15 Scheme of the photocatalytic mechanism of the electron–hole pair separation of $\text{ZrO}_2\text{-ZnO}$ nanoparticles in the degradation of MB

the transfer of holes, contributes to the reduction of the rate of recombination of the electron–hole pairs, a phenomenon that reduces photocatalytic efficiency (Aghabeygi and Khademi-Shamami 2018; Lin et al. 2018).

The photocatalytic decomposition of dye, in this case MB, takes place in stages. Radicals and ions obtained in the photocatalytic process cause the dye to degrade in a multistep process. In the initial stages, the least stable bonds decay, resulting in single ring compounds, which in the final stage become basic inorganic compounds like H_2O , CO_2 , NO_3^- and SO_4^{2-} (Adeleke et al. 2018).

Effect of type of dye on photocatalytic performance

The efficiency of photocatalytic processes depends not only on photocatalyst properties but also on effluent composition, including the type of removed dye. The effect of the composition of the dye mixture on the photocatalytic properties of the deposit was investigated by studies of the photodegradation of a mixture of Methyl Orange (MO) and MB (MB) dye. The UV–Vis spectra of the solutions of the dyes after 30 min of photodegradation are shown in Fig. 16. Based on the UV–Vis spectra, the characteristic wavelengths for each dye were chosen: 464 nm for MO and 664 nm for MB. Analysis of the results showed a much higher amount of degraded MB compared to MO. The amount of degraded MB, which is a cationic dye, remained at 90%, while the amount of degraded MO did not exceed 70% (Table 6).

The higher efficiency of MB removal may result from the presence of an increased amount of $\cdot\text{OH}$ and OH^- groups on the surface of $\text{ZrO}_2\text{-ZnO}$, which interact with positively charged MB ions and cause their decomposition

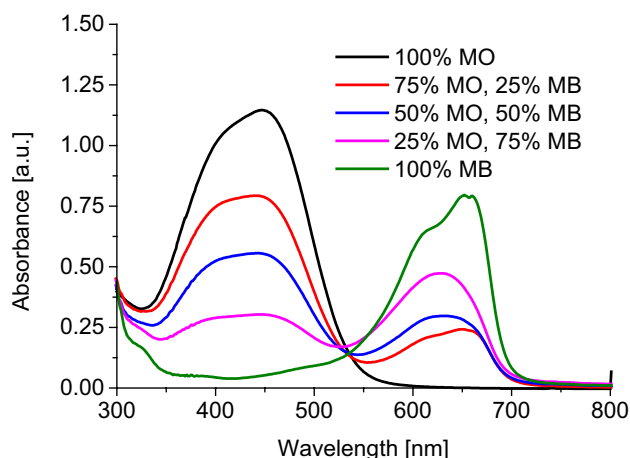


Fig. 16 Interference by mixture of dyes evaluated by UV–Vis spectra after 30 min of photodegradation of solutions of MO and MB in different mass concentrations of each dye: (pure MO) 40 mg/dm^3 , 75% MO–25% MB, 50% MO–50% MB, 25% MO–75% MB, (pure MB) 40 mg/dm^3

rather than the anionic dye. Similar conclusions have been reached by Trandafilović et al. among others, who investigated the effect of the dye type on the efficiency of a ZnO-Eu deposit. They confirmed higher MB removal compared to MO. They also confirmed the significant effect of the presence of OH groups during the removal of MB, while for MO, the most important factor was the formation of holes (Trandafilović et al. 2017). Beura and Thangadurai studied the degradation efficiency of the Sn-ZnO-graphene for mixed dyes (MO and MB). 17% of MO was degraded under UV, whereas MB was

Table 6 Amount of degraded dyes (MB, MO), separated and combined in different proportions

Composition of dyes mixture	The amount of the degraded dye R_D (mg/g)		The total amount of the degraded dyes (mg/g)
	MB	MO	
Methylene Blue 40 mg/dm ³	21.84	–	21.84
75% MB (30 mg/dm ³) + 25% OM (10 mg/dm ³)	17.28	3.70	20.98
50% MB (20 mg/dm ³) + 50% OM (20 mg/dm ³)	11.58	7.57	19.15
25% MB (10 mg/dm ³) + 75% OM (30 mg/dm ³)	5.62	11.57	17.19
Methyl Orange 40 mg/dm ³	–	10.65	10.65

simultaneously degraded with 78% efficiency under UV (Beura and Thangadurai 2018).

Conclusions

ZnO crystallites were successfully synthesised with different amounts of ZrO₂ via a precipitation method with the help of microwave irradiation. Results showed that the addition of ZrO₂ significantly increased the photocatalytic properties of ZnO. Different widths of energy bands occurring in both oxides contributed to reducing the distance between the conduction bands and the valence bands in the whole composite. An increase in the mass of the bed, an increase in the pH of the solution, and a decrease in the initial concentration of MB caused the photocatalytic efficiency of ZrO₂–ZnO to be over 97% after just 30 min. The photocatalytic activity of cationic dye MB was greater than the photodegradation of anionic dye MO.

Funding This research did not receive any specific grant from funding agencies in the public, commercial, or not-for-profit sector.

Compliance with ethical standards

Conflict of interest The authors report no declarations of interest.

Open Access This article is distributed under the terms of the Creative Commons Attribution 4.0 International License (<http://creativecommons.org/licenses/by/4.0/>), which permits unrestricted use, distribution, and reproduction in any medium, provided you give appropriate credit to the original author(s) and the source, provide a link to the Creative Commons license, and indicate if changes were made.

References

Adeleke JT, Theivasanthi T, Thiruppathi M, Swaminathan M, Akomolafe T, Alabi AB (2018) Photocatalytic degradation of methylene blue by ZnO/NiFe₂O₄ nanoparticles. *Appl Surf Sci* 455:195–200. <https://doi.org/10.1016/J.APSUSC.2018.05.184>

Aghabeygi S, Khademi-Shamami M (2018) ZnO/ZrO₂ nanocomposite: sonosynthesis, characterization and its application for

wastewater treatment. *Ultrasonics Sonochem* 41:458–465. <https://doi.org/10.1016/j.ultsonch.2017.09.020>

- Aghabeygi S, Sharifi Z, Molahasani N (2017) Enhanced photocatalytic property of nano-ZrO₂–SnO₂ NPs for photodegradation of an azo dye. *Digest J Nanomater Biostruct* 12. http://www.chalcogen.ro/81_AghabeygiS.pdf. Accessed 4 Sept 2019
- Al-Hamdi AM, Sillanpää M, Dutta J (2015) Gadolinium doped tin dioxide nanoparticles: an efficient visible light active photocatalyst. *J Rare Earths* 33(12):1275–1283. [https://doi.org/10.1016/S1002-0721\(14\)60557-3](https://doi.org/10.1016/S1002-0721(14)60557-3)
- Balcha A, Yadav OP, Dey T (2016) Photocatalytic degradation of methylene blue dye by zinc oxide nanoparticles obtained from precipitation and sol–gel methods. *Environ Sci Pollut Res* 23:25485–25493. <https://doi.org/10.1007/s11356-016-7750-6>
- Bartošová A, Blinová L, Sirotiak M, Michalíková A (2017) Usage of FTIR-ATR as non-destructive analysis of selected toxic dyes. *Res Pap Fac Mater Sci Technol Slovak Univ Technol* 25:103–111. <https://doi.org/10.1515/rput-2017-0012>
- Beura R, Thangadurai P (2018) Effect of Sn doping in ZnO on the photocatalytic activity of ZnO–graphene nanocomposite with improved activity. *J Environ Chem Eng* 6:5087–5100. <https://doi.org/10.1016/J.JECE.2018.07.049>
- Chen X, Zhang F et al (2015) The synthesis of ZnO/SnO₂ porous nanofibers for dye adsorption and degradation. *Dalton Trans* 44:3034–3042. <https://doi.org/10.1039/C4DT03382E>
- Dal Santo V, Naldoni A, Dal Santo V, Naldoni A (2018) Titanium dioxide photocatalysis. *Catalysts* 8:591. <https://doi.org/10.3390/catal8120591>
- Garino N, Limongi T et al (2019) A microwave-assisted synthesis of zinc oxide nanocrystals finely tuned for biological applications. *Nanomaterials* 9:212. <https://doi.org/10.3390/nano9020212>
- Gurushantha K, Renuka L et al (2017) Photocatalytic and photoluminescence studies of ZrO₂/ZnO nanocomposite for LED and Waste water treatment applications. *Mater Today Proc* 4:11747–11755. <https://doi.org/10.1016/j.matpr.2017.09.091>
- Hasanpoor M, Aliofkhaezai M, Delavari H (2015) Microwave-assisted synthesis of zinc oxide nanoparticles. *Procedia Mater Sci* 11:320–325. <https://doi.org/10.1016/J.MSPRO.2015.11.101>
- Ibrahim MM (2015) Photocatalytic activity of nanostructured ZnO–ZrO₂ binary oxide using fluorometric method. *Spectrochim Acta Part A Mol Biomol Spectrosc* 145:487–492. <https://doi.org/10.1016/j.saa.2015.02.057>
- Janaki AC, Sailatha E, Gunasekaran S (2015) Synthesis, characteristics and antimicrobial activity of ZnO nanoparticles. *Spectrochim Acta Part A Mol Biomol Spectrosc* 144:17–22. <https://doi.org/10.1016/J.SAA.2015.02.041>
- Karuppaiah S, Annamalai R et al (2019) Efficient photocatalytic degradation of ciprofloxacin and bisphenol A under visible light using Gd₂WO₆ loaded ZnO/bentonite nanocomposite. *Appl Surf Sci* 481:1109–1119. <https://doi.org/10.1016/j.apsusc.2019.03.178>

- Khan SA, Khan SB, Asiri AM, Ahmad I (2016) Zirconia-based catalyst for the one-pot synthesis of coumarin through Pechmann reaction. *Nanoscale Res Lett*. <https://doi.org/10.1186/s11671-016-1525-3>
- Kokorin AI, Sviridova TV et al (2018) Structure and photocatalytic properties of TiO₂/MoO₃ and TiO₂/V₂O₅ nanocomposites obtained by mechanochemical activation. *Russ J Phys Chem B* 12:330–335. <https://doi.org/10.1134/S1990793118020173>
- Lakshmi C, Ananda S, Rudrappa S, Ranganathaiah C (2012) Synthesis of ZnO/ZrO₂ nanocomposites by electrochemical method and photocatalytic degradation of fast green dye, paper dyeing and printing press effluent. *Int J Mater Sci* 3:221–237
- Lee KM, Abd Hamid SB, Lai CW (2015) Mechanism and kinetics study for photocatalytic oxidation degradation: a case study for phenoxyacetic acid organic pollutant. *J Nanomater* 2015:1–10. <https://doi.org/10.1155/2015/940857>
- Lin J, Luo Z, Liu J, Li P (2018) Photocatalytic degradation of methylene blue in aqueous solution by using ZnO–SnO₂ nanocomposites. *Mater Sci Semicond Process* 87:24–31. <https://doi.org/10.1016/j.MSSP.2018.07.003>
- Lu D, Gao Q, Wu X, Fan Y (2017) ZnO nanostructures decorated hollow glass microspheres as near infrared reflective pigment. *Ceram Int* 43:9164–9170. <https://doi.org/10.1016/j.CERAMINT.2017.04.067>
- Manjunatha S, Dharmaprakash MS (2016) Microwave assisted synthesis of cubic zirconia nanoparticles and study of optical and photoluminescence properties. *J Lumin* 180:20–24. <https://doi.org/10.1016/j.jlumin.2016.07.055>
- Mexicana De Física S, México AC et al (2007) Use of diffuse reflectance spectroscopy for optical characterization of un-supported nanostructures. *Revista Mexicana De Física S* 53. <http://www.redalyc.org/articulo.oa?id=57028299004>. Accessed 4 Sept 2019
- Nagao T, Dao TD, Sugavaneshwar RP, Chen K, Nanda KK (2016) Effects of nanoscale morphology and defects in oxide: optoelectronic functions of zinc oxide nanowires. *Radiat Eff Defects Solids* 171:22–33. <https://doi.org/10.1080/10420150.2016.1160906>
- Oluwabi AT, Acik IO, Katerski A, Mere A, Krunk M (2018) Structural and electrical characterisation of high-k ZrO₂ thin films deposited by chemical spray pyrolysis method. *Thin Solid Films* 662:129–136. <https://doi.org/10.1016/j.TSF.2018.07.035>
- Payra S, Challagulla S, Bobde Y, Chakraborty C, Ghosh B, Roy S (2019) Probing the photo- and electro-catalytic degradation mechanism of methylene blue dye over ZIF-derived ZnO. *J Hazard Mater* 373:377–388. <https://doi.org/10.1016/j.JHAZMAT.2019.03.053>
- Pirzada BM, Mir NA, Qutub N, Mehraj O, Sabir S, Muneer M (2015) Synthesis, characterization and optimization of photocatalytic activity of TiO₂/ZrO₂ nanocomposite heterostructures. *Mater Sci Eng B* 193:137–145. <https://doi.org/10.1016/j.MSEB.2014.12.005>
- Qiu L, Gong ZY, Li HL, Ouyang F (2018) Stably photocatalytic decomposition of rhodamine-B by samarium doped ZrO₂–ZnO composite under simulant solar light irradiation. In: Proceedings of the 2018 international conference on energy development and environmental protection (EDEP 2018), Paris, France. Atlantis Press. <https://doi.org/10.2991/edep-18.2018.2>
- Reszczyńska J, Grzyb T, Sobczak JW, Lisowski W, Gazda M, Ohtani B, Zaleska A (2015) Visible light activity of rare earth metal doped (Er³⁺, Yb³⁺ or Er³⁺/Yb³⁺) titania photocatalysts. *Appl Catal B* 163:40–49. <https://doi.org/10.1016/j.apcatb.2014.07.010>
- Ruiz-Hitzky E, Aranda P, Akkari M, Khaorapong N, Ogawa M (2019) Photoactive nanoarchitectures based on clays incorporating TiO₂ and ZnO nanoparticles. *Beilstein J Nanotechnol* 10:1140–1156. <https://doi.org/10.3762/bjnano.10.114>
- Sapawe N, Jalil AA, Triwahyono S (2013) One-pot electro-synthesis of ZrO₂–ZnO/HY nanocomposite for photocatalytic decolorization of various dye-contaminants. *Chem Eng J* 225:254–265. <https://doi.org/10.1016/j.cej.2013.03.121>
- Singh AK, Nakate UT (2014) Microwave synthesis, characterization, and photoluminescence properties of nanocrystalline zirconia. *Sci World J* 2014:1–7. <https://doi.org/10.1155/2014/349457>
- Sowik J, Miodyńska M et al (2019) Optical and photocatalytic properties of rare earth metal-modified ZnO quantum dots. *Appl Surf Sci* 464:651–663. <https://doi.org/10.1016/j.APSUSC.2018.09.104>
- Spathis P, Poullos I (1995) The corrosion and photocorrosion of zinc and zinc oxide coatings. *Corros Sci* 37:673–680. [https://doi.org/10.1016/0010-938X\(95\)80001-8](https://doi.org/10.1016/0010-938X(95)80001-8)
- Thirumalai K, Shanthi M, Swaminathan M (2017) Synthesis and characterization of gadolinium tungstate doped zinc oxide photocatalyst. *Indian J Chem Sect A Inorg Phys Theor Anal Chem* 56A:50–56
- Trandafilović LV, Jovanović DJ, Zhang X, Ptašíńska S, Dramićanin MD (2017) Enhanced photocatalytic degradation of methylene blue and methyl orange by ZnO: Eu nanoparticles. *Appl Catal B* 203:740–752. <https://doi.org/10.1016/j.APCATB.2016.10.063>
- Uribe López MC, Alvarez Lemus MA et al (2019) Synthesis and characterization of ZnO–ZrO₂ nanocomposites for photocatalytic degradation and mineralization of phenol. *J Nanomater* 2019:1–12. <https://doi.org/10.1155/2019/1015876>
- Zinatloo-Ajabshir S, Salavati-Niasari M (2016) Facile route to synthesize zirconium dioxide (ZrO₂) nanostructures: structural, optical and photocatalytic studies. *J Mol Liq* 216:545–551. <https://doi.org/10.1016/j.MOLLIQ.2016.01.062>

Publisher's Note Springer Nature remains neutral with regard to jurisdictional claims in published maps and institutional affiliations.